

PHASE-DEPENDENT PHOTOMETRIC AND SPECTROSCOPIC CHARACTERIZATION OF THE
MASTER-NET OPTICAL TRANSIENT J212444.87+321738.3: AN OXYGEN RICH MIRA

SUPRIYO GHOSH,¹ SOUMEN MONDAL,¹ RAMKRISHNA DAS,¹ D. P. K. BANERJEE,² N.M. ASHOK,² FRANZ-JOSEF HAMBSCH,^{3,4}
AND SOMNATH DUTTA¹

¹*S. N. Bose National Centre for Basic Sciences, Salt Lake, Kolkata-700 106, India*

²*Physical Research Laboratory, Navrangpura, Ahmedabad-380 009, India*

³*Vereniging Voor Sterrenkunde (VVS), Brugge, BE-8000, Belgium*

⁴*American Association of Variable Star Observers (AAVSO), Cambridge, USA*

(Received ; Revised; Accepted)

Submitted to ApJ

ABSTRACT

We describe the time-dependent properties of a new spectroscopically confirmed Mira variable, which was discovered in 2013 as MASTER-Net Optical Transient (OT) J212444.87+321738.3 towards the Cygnus constellation. We have performed long-term optical/near-infrared (NIR) photometric and spectroscopic observations to characterize the object. From the optical/NIR light curves, we estimate a variability period of 465 ± 30 days. The wavelength-dependent amplitudes of the observed light-curves range from $\Delta I \sim 4$ mag to $\Delta K \sim 1.5$ mag. The (J-K) color-index varies from 1.78 to 2.62 mag over phases. Interestingly, a phase lag of ~ 60 days between optical and NIR light curves is also seen, as in other Miras. Our optical/NIR spectra show molecular features of TiO, VO, CO, and strong water bands which are a typical signature of oxygen-rich Mira. We rule out S- or C-type as ZrO bands at 1.03 and $1.06 \mu\text{m}$ and C_2 band at $1.77 \mu\text{m}$ are absent. We estimate the effective temperature of the object from the SED, and distance and luminosity from standard Period-Luminosity relations. The optical/NIR spectra display time-dependent atomic and molecular features (e.g. TiO, NaI, CaI, H₂O, CO), as commonly observed in Miras. Such spectroscopic observations are useful for studying pulsation variability in Miras.

Keywords: Red giants — Long period variable — AGB — Mira — O-rich

1. INTRODUCTION

Mira-type variables are in the Asymptotic giant branch (AGB) phase, which is the last stage of stellar evolution before turning into planetary nebulae. Miras are long-period (100–1000 days) pulsating variable with a large visible amplitude of more than 2.5 mag. These giants have initial masses $\approx 0.8\text{--}8 M_{\odot}$ (low to intermediate main sequence mass), and are generally surrounded by circumstellar matter from huge mass loss rates of $\sim 10^{-8} - 10^{-4} M_{\odot} \text{ yr}^{-1}$ (Jura & Kleinmann 1990; Habing 1996; Mattei 1997; Olofsson 2004; Herwig 2005). Mira variables have a low effective temperature (< 3500 K), cool extended atmospheres (radius up to few $100R_{\odot}$), and luminosity can reach up to a few $10^3 L_{\odot}$ (Mattei 1997). High luminous Mira variables play a significant role in the studies of stellar evolution, stellar populations, galactic- extragalactic structure and evolution (Lançon et al. 1999; Dejonghe & van Caelenberg 1999; Groenewegen et al. 2009), and enriches the interstellar medium (ISM) significantly through the high mass-loss (Habing 1996). The high mass loss and relatively low surface temperature of these evolved stars provide a habitable zone for several molecules such as TiO, VO, H_2O , and CO in their extended atmospheres. These molecules play important roles in the spectral appearance of Mira variable stars at visual and NIR wavelengths (Lançon & Wood 2000; Gautschy–Loidl et al. 2004; Aringer et al. 2009; Nowotny et al. 2010).

The stars in the AGB phase are radially pulsating and become unstable. Mira variables are thought to be fundamental mode pulsators (e.g., Wood et al. 1999; Ita et al. 2004). The pulsation mode of Miras is a function of period, mass and radius (Wood & Sebo 1996). The Mira pulsation is thought to be originating from the variable ionization zone of hydrogen and helium below the stellar surface (e.g., Keeley 1970). From each pulsation cycle, shock waves are generated under the photospheric surface, which in turn create a very complex and dynamic atmosphere (Reid & Goldston 2002). The photometric light curves of Mira variables represent the oscillating behavior of brightness, surface temperature, radius, atmospheric structure and opacity as the star pulsates (Le Bertre 1992; Castelaz et al. 2000). The significant visual variation is attributed to the opacity variation of metal oxides in the Mira atmosphere (Reid & Goldston 2002). The observed radii of Mira stars significantly differ at different optical/NIR wavelengths as seen from high angular resolution observations (e.g., Thompson et al. 2002; Ireland et al. 2004; Perrin 2004; Mondal et al. 2005). These results indicate the presence of molecular layers above the continuum-forming photosphere (Wittkowski et al. 2008). The

theoretical hydrodynamic pulsation models have been developed to understand the pulsation and mass loss mechanisms, which can predict the time-dependent structure and temporal variations over multiple cycles (Fleischer et al. 1992; Bessell, Scholz & Wood 1996; Winters et al. 1997; Höfner et al. 1998; Loidl et al. 1999; Winters et al. 2000; Tej et al. 2003a). These models are characterized by pulsation-driven shocks, non-equilibrium chemistry, and formation of dust grains (Bieging et al. 2002).

Spectroscopic observational studies are valuable tools to understand pulsating atmospheres and mass loss of Mira variables throughout the outer layer (Hinkle et al. 1982; Alvarez et al. 2000; Castelaz & Luttermoser 1997; Castelaz et al. 2000; Lançon & Wood 2000; Tej et al. 2003b). Phase-dependent spectroscopic studies are very efficient to probe the atmosphere of the stars, and such studies are limited in the literature. From radial velocity, excitation temperatures and lines broadening measurements using high resolution spectroscopy, it is evident that two separate line forming regions of the atmosphere sometimes contribute towards the spectrum of H_2O (except maximum light), CO ($\Delta\nu = 2$), and OH (Hinkle 1978; Hinkle & Barnes 1979a; Nowotny et al. 2010). More complex stratification may also exist (e.g., Tej et al. 2003a; Tsuji 2009).

In this paper, we have studied an object, which was first detected from MASTER Optical Transient (OT) alert on J212444.87+321738.3 (hereafter, J2124+32) on 2013 March 13 with 10.7 mag at unfiltered CCD (Tiurina et al. 2013). The Mobile Astronomical System of Telescope Robots (MASTER) Global Robotic Net¹ consists of several identical observing instruments at different observatories (e.g., MASTER-Amur, MASTER-Tunka, MASTER-SAAO). The facilities provide very fast sky-survey (128 deg^2 per hour) with limiting magnitude 19–20 (Lipunov et al. 2016, 2017). The primary goals of the MASTER-net are to observe gamma-ray bursts (GRB) in alert mode. However, it discovers many OTs in the survey mode. The other identification of object are USNO-B1.0 1222-0647260, 2MASS 21244500+3217377 and WISE J212444.98+321737.73.440 (Tiurina et al. 2013). Following the OT announcement, we have started spectrophotometric monitoring observations on the object in optical/NIR wavelength since 2013 March 20 for more than 1.5 years using different telescope facilities. We present here the result of characterization MASTER OT J2124+32, which turns out to be a new O-rich

¹ <http://observ.pereplet.ru/>

Mira variable. From the 3rd and 4th edition of General Catalog Variable Stars, galactic Mira detection limit is complete down to maximum magnitude $V \approx 9$ mag. (Kharchenko et al. 2002). This new Mira variable has a peak magnitude at I-band ≈ 10.4 mag, which corresponds to $V \approx 14$ (Kharchenko et al. 2002). Because of faintness, the object might not be included in the variability monitoring program. The paper is organized as we describe the details of our observations and data reduction procedures in section II and section III deals with our new results and discussion. Finally, the summary and conclusion of our studies are mentioned in section IV.

2. OBSERVATIONS AND DATA REDUCTION

Optical imaging observations of J2124+32 were performed using a front-illuminated $4K \times 4K$ CCD camera on the 40 cm f/6.8 Optimized Dall Kirkham (ODK) telescope at the private observatory ROAD (Remote Observatory Atacama Desert) in Chile (Hambsch 2012). The source was monitored in optical I-band and unfiltered CCD (400–900 nm) filter-band (Clear, C) over 550 days during 2013 April 02 to 2014 August 31. The accuracy of these observations varies from 0.004 at I=10.40 to 0.047 at I=14.30, while from 0.007 at C= 12.35 to 0.045 at C=15.70 mag respectively.

The NIR photometric and spectroscopic observations were carried out using Near-Infrared Imaging Camera cum Multi-Object Spectrograph (NICMOS-3) on 1.2m Mt. Abu telescope, India, and TIFR Near-Infrared Spectrometer and Imager (TIRSPEC) on 2m Himalayan Chandra Telescope (HCT) at Hanle, India. The NICMOS3 has 256×256 HgCdTe detector array and provides a resolution $R \approx 1000$; while TIRSPEC has 1024×1024 Hawaii-1 array and provides resolution $R \approx 1200$. The spectral coverage of NICMOS-3 were on *JHK*-bands. The spectrograph in the NICMOS-3 instrument does not cover the whole K-band in a single shot. We observed in two parts, the 1st part covers 1.9–2.3 μm (termed as K), and the 2nd part covers 2.1–2.4 μm with some overlap (termed as KA). The TIRSPEC spectra were taken at *YJHK* bands. More details of TIRSPEC could be found elsewhere (Ninan et al. 2014). Photometric observations in *JHK'*-bands were taken in five dithered positions, and multiple frames are taken in each dithered position to get better signal to noise ratio (SNR). In spectroscopic observing mode, the spectra were taken at two different positions along the slit one after another immediately to subtract the sky, and several frames were observed to improve SNR. We have estimated the SNR of our spectra. The SNR is ~ 50 (J-band), ~ 80 (H-band), ~ 80 –100 (K-band) for TIRSPEC

data. While the SNR is ~ 30 (JHK) for NICMOS-3 data. A log of our observations is mentioned in Table 1.

The optical spectra are taken using Himalaya Faint Object Spectrograph and Camera (HFOSC) on the 2m HCT at Hanle, India. The HFOSC instrument has several gratings covering different wavelength range and resolution, and we have used Grism no. 8 (Gr#8) for our studies, which covers the wavelength range of 580–920 nm respectively and provides a resolution $R \approx 2200$ ².

The data reduction was performed with the help of standard tasks of the Image Reduction and Analysis Facility (IRAF³). In NIR photometric reduction, the sky frames were generated with all dithered frames by median combining and subtracted from object frames. In Optical photometric reduction, bias-correction, flat-fielding, and removal of cosmic rays were done on raw images to clean the science frames. The aperture photometry was carried out with these processed images using APPHOT package of IRAF. The zero-points of photometry were determined using the standard stars.

The spectroscopic analysis was done using APALL task of IRAF. The TIRSPEC data was reduced with TIRSPEC pipe-line⁴ (Ninan et al. 2014), and is cross-checked with the IRAF reduction. Both techniques agree well. The wavelength calibration in NICMOS-3 data was performed using OH skylines, while Argon lamp is used for TIRSPEC data. The wavelength calibration of optical spectra (HFOSC data) was done by using a FeNe arc spectrum. The science frames are divided by a standard star, observed at the similar airmass as science target, to remove the telluric features of the Earth's atmosphere. Then the flux calibration of the target stars is performed using the standard star.

3. RESULT AND DISCUSSION

3.1. Optical Light Curves and Period

Fig. 1 shows the optical light curves in I-band and unfiltered (400–900 nm) CCD (Clear, C). The amplitudes of optical variability are estimated to be ~ 4.00 mag, and ~ 3.4 mag in I band and unfiltered CCD respectively. Such large amplitude of variability with a long-term period is only observed in a case of Mira-like variables (Whitelock et al. 2003). The general criteria to be a Mira variable, the amplitude variability in I-band should be greater than 1.0 mag (Soszyński et al. 2012).

² https://www.iap.res.in/iao_hfosc

³ <http://iraf.noao.edu/>

⁴ <https://github.com/indiajoe/TIRSPEC/wiki>

Table 1. Log of photometric and spectroscopic observations

Date of Observation	Observation Type	Spectral Band	Int. Time (s)	No of Frames	Telescope	Remarks
2013-Mar-20	Photometry	J/H/K	0.4/0.2/0.2	5* [21/21/21]	1.2m Mt. Abu	clear sky
2013-Mar-22	Photometry	J/H/K	0.5/0.4/0.2	5* [11/11/21]	1.2m Mt. Abu	clear sky
2013-Apr-28	Photometry	J/H/K	2/1/0.3	5* [15/15/25]	1.2m Mt. Abu	clear sky
2013-Apr-29	Photometry	J/H/K	0.5/0.5/0.2	5* [31/31/31]	1.2m Mt. Abu	clear sky
2013-May-27	Photometry	J/H/K	0.3/0.7/1	5* [15/15/35]	1.2m Mt. Abu	clear sky
2013-May-28	Photometry	J/H/K	1/1/0.3	5* [21/21/35]	1.2m Mt. Abu	clear sky
2013-May-30	Photometry	J/H/K	0.3/0.5/1	5* [15/15/15]	1.2m Mt. Abu	clear sky
2013-Jun-20	Photometry	J/H/K	0.3/0.5/1	5* [15/15/15]	1.2m Mt. Abu	clear sky
2013-Oct-30	Photometry	J/H/K	0.3/0.5/1	5* [15/15/15]	1.2m Mt. Abu	clear sky
2015-May-08	Photometry	J/H/K	0.3/0.5/1	5* [15/15/15]	1.2m Mt. Abu	clear sky
2013-Apr-02 - 2014-Aug-31	Photometry	I/CV	60/30	515/515	40cm Chile	—
2013-Mar-20	Spectroscopy	J/H/K/KA	120/90/60/60	2*1	1.2m Mt. Abu	clear sky
2013-Apr-28	Spectroscopy	J/H/K/KA	90/75/60/60	2*1	1.2m Mt. Abu	clear sky
2013-May-30	Spectroscopy	J/H/K/KA	90/60/60/60	2*1	1.2m Mt. Abu	clear sky
2013-Oct-15	Spectroscopy	600-920 <i>nm</i>	1800	1	2m HCT	clear sky
2014-May-21	Spectroscopy	600-920 <i>nm</i>	300	1	2m HCT	clear sky
2014-Aug-18	Spectroscopy	H/K	30/30/20/10	2*5	2m HCT	clear sky
2014-Aug-19	Spectroscopy	600-920 <i>nm</i>	300	1	2m HCT	clear sky
2014-Oct-06	Spectroscopy	YJ/HK	100/100	2*7	2m HCT	clear sky
		600-920 <i>nm</i>	600	1		
2014-Dec-12	Spectroscopy	YJ/HK	100/100	2*7	2m HCT	clear sky
		600-920 <i>nm</i>	600	1		
2015-Jan-13	Spectroscopy	YJ/HK	100/100	2*7	2m HCT	clear sky
2015-Jan-18	Spectroscopy	600-920 <i>nm</i>	900	1	2m HCT	clear sky
2015-July-05	Spectroscopy	YJ/HK	100/100	2*5	2m HCT	clear sky
		600-920 <i>nm</i>	1	1		
2015-Aug-11	Spectroscopy	YJ/HK	100/100	2*5	2m HCT	clear sky
2016-Dec-19	Spectroscopy	HK	100	2*5	2m HCT	clear sky

For determination of the period of this object, we used the Lomb-Scargle (LS) periodogram (Lomb 1976; Scargle 1982), the algorithm publicly available at the starlink⁵ software database. The LS method is used to find out significant periodicity even with unevenly sampled data and verified successfully in several cases to determine periods from such sparse data sets (Mondal et al. 2010). The left bottom panel of Fig. 1 shows the periodograms of the light curves determined from the LS method. We found the period to be 512 ± 100 days, and significant uncertainty in period is due

to limited time coverage, which is not cover a complete periodic cycle. The period is also verified from PERIOD04⁶ (Lenz & Breger 2005), which provides the same result.

As noted in (Lebzelter et al. 1999), the classical method for deriving a period using Fourier analysis like LS method do not always provide satisfying results for light curves of AGB variables. Alternatively, we have used Fourier decomposition technique with the fitting of the following function as in Ngeow et al. (2013),

⁵ <http://starlink.eao.hawaii.edu/starlink>

⁶ <http://www.univie.ac.at/tops/Period04>

Table 2. Near-IR JHK' Photometry

Date of Obs. (UT)	Optical Phase	Telescope/Instrument	J (mag)	H (mag)	K (mag)	(J-K) (mag)
2013 Mar 22.02	0.049	Mt. Abu/NICMOS-3	5.852 ± 0.055	4.467 ± 0.062	3.765 ± 0.049	2.087
2013 Mar 24.01	0.051	Mt. Abu/NICMOS-3	5.642 ± 0.044	4.483 ± 0.035	3.765 ± 0.034	1.877
2013 Apr 28.93	0.118	Mt. Abu/NICMOS-3	5.668 ± 0.043	4.654 ± 0.052	3.751 ± 0.010	1.917
2013 Apr 29.98	0.119	Mt. Abu/NICMOS-3	5.557 ± 0.021	4.510 ± 0.023	3.720 ± 0.012	1.837
2013 May 27.92	0.169	Mt. Abu/NICMOS-3	5.621 ± 0.051	4.466 ± 0.063	3.827 ± 0.045	1.794
2013 May 28.95	0.170	Mt. Abu/NICMOS-3	5.718 ± 0.047	4.452 ± 0.053	3.752 ± 0.048	1.966
2013 Jun 20.83	0.213	Mt. Abu/NICMOS-3	5.807 ± 0.034	4.621 ± 0.024	4.021 ± 0.029	1.786
2013 Oct 30.50	0.450	Mt. Abu/NICMOS-3	7.110 ± 0.020	5.660 ± 0.030	4.850 ± 0.020	2.260
2015 May 08.91	1.60	Mt. Abu/NICMOS-3	7.868 ± 0.017	6.426 ± 0.06	5.243 ± 0.015	2.625
1998 Jun 18.00 ^a		2MASS/NICMOS	7.825 ± 0.026	5.971 ± 0.017	4.818 ± 0.015	3.007
Average		Mt. Abu/NICMOS3	6.093 ± 0.257	4.859 ± 0.220	4.077 ± 0.17	2.016
Amplitude (light curve)		Mt. Abu/NICMOS3	2.2	1.9	1.5	

^aCutri et al. (2003)

$$m(t) = A_0 + \sum_{\kappa=1}^N A_{\kappa} \sin(\kappa\omega t + \phi_{\kappa}) \quad (1)$$

Where $\omega = 2\pi/P$, P is the period in days, A_{κ} and ϕ_{κ} represent the amplitude and phase-shift for κ^{th} -order respectively, and N is the order of the fit. To fit the light curve, we use up to third order terms. From χ^2 minimization technique, we find the best fitted period of 465 ± 30 days on our light curves. The solid black line is the Fourier fit which is shown in Fig. 1 along with observed data in the respective panels. The estimated period of this red object is consistent with red LMC Miras ($J-K \geq 2.08$) having periods of 300–500 days (Ita et al. 2004).

3.2. Near-Infrared light curves

NIR JHK' -bands photometric observations were carried out during 20 March 2013 to 09 May 2015 in a sparse sampling of the Mira cycle, and JHK' magnitudes are listed in Table 2. Our JHK' magnitudes on first two epoch are reported immediately at ATEL (Mondal et al. 2013). The NIR JHK' light curves are shown in the right panels of Fig. 1. For comparison, the optical I-band light curve is also overplotted on those NIR light curves after scaling with JHK' magnitudes. The light curve is fitted to the Eqn. 1 mentioned above with the same period of the optical light curve fit. The amplitudes (peak to peak) of the variability are estimated from our light curves to be $\Delta J \sim 2.2$ mag, $\Delta H \sim 1.9$ mag and $\Delta K \sim 1.5$ mag respectively. These op-

tical/NIR light curves confirm typical Mira behavior of strong wavelength dependence, i.e., the pulsation amplitude decreases with increasing wavelength (Smith et al. 2002). Bessell, Scholz & Wood (1996) showed that colors such as V-K change much more with phase than near-IR colors (e.g., (J-H), (H-K), (J-K)), which is another way of saying that visual amplitudes are larger than near-IR amplitudes. The fact that the pulsation amplitude decreases with increasing wavelength is a result of the changes in T_{eff} that accompany the changes in luminosity, and is exacerbated by the dependence of TiO opacities on temperature. Another interesting feature, a phase lag of about 60 days, corresponding to ~ 0.13 of phase, between the optical and NIR maxima or minima is observed here in Fig. 1, which is seen in Mira variables (Smith et al. 2002). Such phase lag in oxygen-rich Miras may be due to the opacity of TiO molecules in their atmosphere (Smith et al. 2006), and even large visual amplitude might be due to formation and destruction of TiO molecules during the passage of periodic shock waves (Reid & Goldston 2002). The 2MASS (J-K) colour is 3.0 mag (Cutri et al. 2003). We also find a large (J-K) color index, ranging from 1.78 to 3.0 mag (Table 2), which are again consistent with the source being an extreme red Mira variable (Ita et al. 2004; Whitelock, Marang & Feast 2000). We rule out the object is a semi-regular variables as the latter are not this red.

3.3. Distances and Luminosity

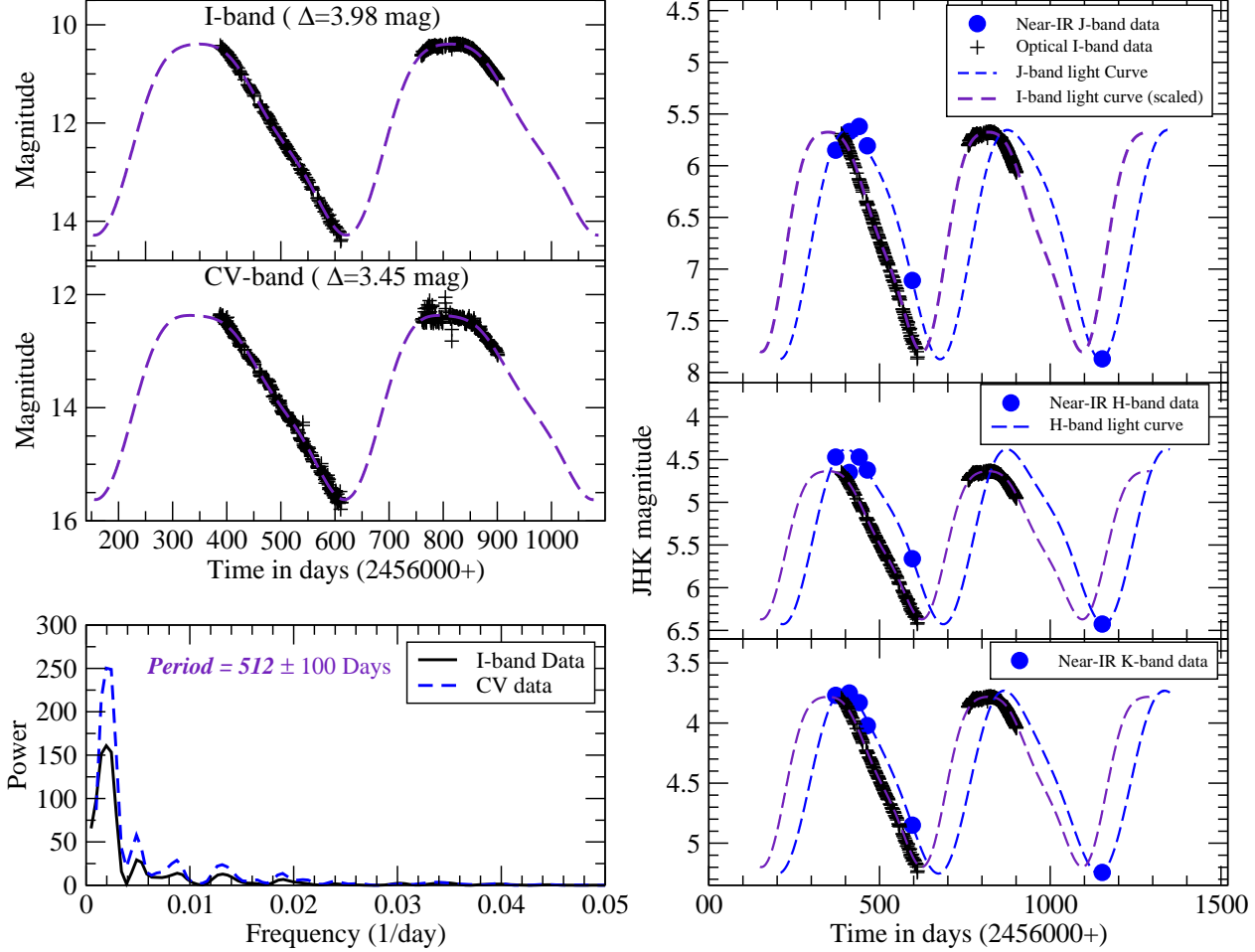


Figure 1. The left figures show the optical light curves of J2124+32 with fitting using Eqn. 1 in I-band (left top) and unfiltered CCD in 400–900 nm (C) (left middle). The periodograms of optical light curves are shown in the left bottom panel. The NIR JHK light curves of J2124+32 are shown in the right three panels (JHK'), where the filled circles are our observed NIR data points, while the solid lines are fitted light curve with $P=465$ days. The optical I-band light curve (scaled with NIR light curves) is over-plotted on NIR light curves for comparison.

To estimate the distance to the source, we have used the period–luminosity (PL) relation for the Miras based on the distance modulus of the Large Magellanic Cloud (LMC) to be 18.50 ± 0.02 , the PL relation is taken from [Ita & Matsunaga \(2011\)](#) expressed as

$$M_K = (-3.675 \pm 0.076) \log P + (1.456 \pm 0.173) \quad (2)$$

According to the relation, the absolute K-band magnitude of the source is estimated to be $M_K = -8.34 \pm 0.34$ mag. We have also examined other available PL relations in [Feast et al. \(1989\)](#) and [Whitelock et al. \(2008\)](#), and the value of M_K is within uncertainty limit. The Galactic interstellar extinction in the direction of the source is $A_V=0.57$ ($A_K=0.05$; [Schlafly et al. 2011](#)) or $A_V=0.68$ ($A_K=0.06$; [Schlegel et al. 1998](#)). Taking $A_K=0.05$, we have obtained the distance (d) to the object, 3.27 ± 0.02 kpc using the relation $m_k - M_K =$

$5 \log d - 5 + A_K$. The uncertainties in the distance measurement come from the estimated period, PL relation and photometric error of calculating K-band magnitude. We have also estimated bolometric magnitude M_{bol} using the following PL relation for Miras ([Hughes & Wood 1990](#)).

$$M_{bol} = -3.22 - 7.76[\log(P/day) - 2.4] \pm 0.38 \quad (3)$$

We have estimated the bolometric magnitude of $M_{bol} = -5.29 \pm 0.38$ corresponding to luminosity $\sim 10250 L_\odot$, which is consistent with other PL relation of [Feast et al. \(1989\)](#). The O-rich Miras with $P \geq 420$ d are over luminous ([Feast et al. 1989](#); [Hughes & Wood 1990](#)), which is consistent with our result. [Feast et al. \(1989\)](#) showed that for few Miras which have periods > 420 d are 0.7 mag brighter than expected extrapolation of PL relation. Also, [Whitelock et al. \(2003\)](#) suggested that Mi-

ras with periods > 400 d have higher luminosities due to hot bottom burning. Putting our object on the Mass-Luminosity relation Fig. 6 of Hughes & Wood (1990), the object with $P=465$ d and $M_{bol}=-5.29$ lies between the mass (M) range of $1.0M_{\odot} - 1.5M_{\odot}$.

To understand the galactic location of the new mira variable, we have estimated the scale height of the object from the distance above the galactic plane (Z) following Jura & Kleinmann (1992). We find that the scale height of the object is about 270 pc which agree with the thin disk population as given by Habing (1988); Jura & Kleinmann (1992); Eggen (1998); Jurić et al. (2008).

3.4. Spectral Energy Distribution

We use near to far infrared multi-wavelength photometric data to generate the spectral energy distribution (SED) of the source J2124+32. The fluxes, used here for the SED fit, are taken from our JHK' measurements and archival mid to far Infrared catalogs. The mean JHK' are estimated from the NIR light curves. The mid-IR 3.35, 11.6, and 22.1 μm data are taken from AllWISE Data Release (Cutri et al. 2013); 8.61, 18.4 μm from AKARI/IRC all-sky Survey (ISAS/JAXA, 2010) (Ishihara et al. 2010); 12, 25 μm from IRAS Faint Source Catalog (IPAC 1992) and Far-IR 65, 90 μm data from AKARI/FIS; 60 μm from IRAS. The observed JHK' magnitudes are converted to flux densities using the zero magnitudes flux from (Bessell et al. 1998).

The radiative transfer code, More of Dusty⁷ (MoD), developed by (Groenewegen 2012), was used to model the dusty circumstellar shell of Mira variable. The MoD is a modified version of a publicly available 1D dust radiative transfer code, "DUSTY" version 2.01 (Ivezić et al. 1999). The detail mathematical formulation of "DUSTY" was described elsewhere (Ivezić & Elitzur 1997). The MoD works to find best-fitted parameters, e.g., luminosity (L), dust optical depth ($\tau_{0.55}$), dust temperature at the inner radius (T_c) and slope of the density law (p), etc. in the minimization process. The quality of the fit is obtained through a χ^2 analysis.

The interstellar reddening (A_V), hydrostatic model atmosphere, the effective temperature of the model atmosphere, distance (D), outer radius in a unit of inner radius, dust properties, etc. are provided as an input in the master-input file. The adopted dust species are taken as mixture of $\text{Mg}_{0.8}\text{Fe}_{1.2}\text{SiO}_4:\text{AlO}:\text{Fe}=100:0:5$, calculated using the distribution of hollow spheres (DHS) with a mean grain size $a=0.15 \mu\text{m}$ and a max-

imum volume fraction of a vacuum core $f_{max}=0.7 \mu\text{m}$ (private communication with M. A. T. Groenewegen). We adopted such dust composition because our spectroscopic studies concluded that the star is O-rich as will be discussed in subsequent sections. The MARCS⁸ hydrostatic model atmospheres (Gustafsson et al. 2008) were used for the spectra of the central stars. The outer radius is set to 1600 times the inner radius, where dust temperature becomes approximately 20 K. In the model, the distance (d) of 3.27 kpc and A_V were adopted as an input to the standard model as discussed in the previous section. The L , τ , T_c and p could be fitted or set to a fixed value.

To get the best fit of photometric data, we generated multiple SEDs considering MARCS model atmospheres of temperature range 2600-3600 K in step of 200 K and setting other free parameters (e.g., L , $\tau_{0.55}$, T_c , p) either fixed or variable as listed in Table 3. The model provides minimum reduced χ^2 value at MARCS model atmospheres of temperature 2800 K, and the parameters of MoD fitting at that temperature for different cases are given in Table 3. Our best fit SED of all photometric measurements for various cases are shown in Fig. 2. We got the minimum value of reduced χ^2 , when all the parameters set free. The χ^2 of the fit is typically large as we include significant JHK' variability in our SED fit, and non-simultaneous taking of the photometric data. The provided errors are therefore internal errors scaled to a reduced χ^2 of 1 (private communication with M. A. T. Groenewegen). The best-fitted SED provides $L=9282 \pm 1590 L_{\odot}$ that is comparable to our P-L based estimation in the earlier section, $\tau=11.178 \pm 3.975$, $T_c=1248 \pm 511$ K and $p=1.75 \pm 0.28$. The best-fit parameters, dust properties and actual grain size translate into a current mass-loss rate of $0.7 \times 10^{-6} M_{\odot} \text{yr}^{-1}$ by assuming a dust-to-gas ratio of 0.005 and an expansion velocity of 10 km/s.

3.5. Optical/NIR spectroscopic studies

Multi-epoch optical/NIR spectroscopic studies on Mira variables at different variability phases probe the dynamic stellar atmosphere and help us also to understand the pulsational related variations of fundamental parameters. The visual spectra of the object taken at several variability phases are shown in Fig. 3. The optical spectra are dominated by molecular absorption bands of TiO and VO in the wavelength range of 7000 to 9000 Å like red M stars (Castelaz et al. 2000; Rayner et al. 2009; Bessell et al. 1989; Fluks et al. 1994). Visual comparison shows that all the optical

⁷ <http://homepage.oma.be/marting/codes.html>

⁸ <http://marcs.astro.uu.se/>

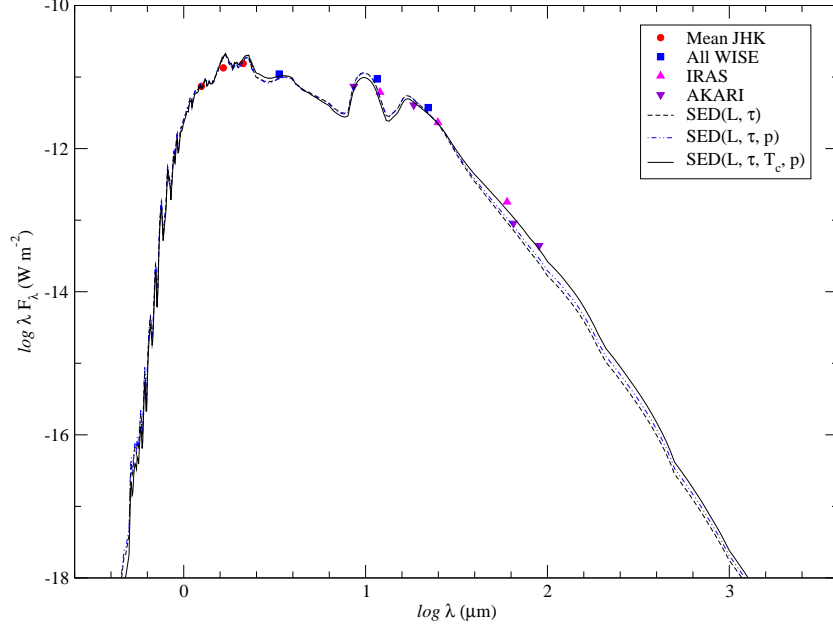


Figure 2. The SED of the target is shown here using multiwavelength data from NIR to far-IR, while the insets show different data source, e.g., our mean JHK', All WISE, AKARI, IRAS data. The SED (L, τ) means fitted SED with L, τ as variables and T_c, p fixed. Similarly for SED(L, τ, p) and SED(L, τ, T_c, p).

Table 3. MoD Models for J2124+32 for three different cases.

Star	L (L_{\odot})	$\tau_{0.55}$	T_c [K]	p	χ^2_{red} ^a	Remarks
	9331 ± 1545	10.064 ± 2.489	1000 fixed	2.0 fixed	819	T_c, p fixed
J2124+32	9255 ± 1659	9.913 ± 2.746	1000 fixed	1.95 ± 0.29	818	T_c fixed
	9282 ± 1590	11.178 ± 3.975	1248 ± 511	1.75 ± 0.28	806	All free

^a χ^2_{red} = reduced χ^2 for the fit of photometric data

spectra of the MASTER OT object correspond to O-rich spectral types later than M7.

The NIR spectra were taken immediately after transient alert of [Tiurina et al. \(2013\)](#) and continued over several variability phases as listed in Table 1. The JHK spectra are shown in Fig. 4. Molecular features of TiO and VO bands dominate in the J-band spectra as shown in the 1st panel of Fig. 4. But no ZrO twin features at 1.03, and 1.06 μm is seen here, which is a primary indicator for S-type Mira stars ([Hinkle et al. 1989](#); [Wright et al. 2009](#)). The most prominent feature of VO band is seen in one of our spectra, which covers from 1.02 μm , which signifies it's oxygen-rich M-type star ([Wright et al. 2009](#)).

In the 2nd panel of Fig. 4, the H-band spectra show the ^{12}CO second overtone series at 1.5582, 1.5780, 1.5982, 1.6189, 1.6397, 1.6610, 1.6840, 1.7067 μm including OH molecular bands all over the band ([Rayner et al. 2009](#)). These second overtone series develop at the objects having a photospheric temperature of ≤ 5000 K,

and their strength is dependent on the photospheric temperatures ([Lançon et al. 2007](#)). The OH molecular bands are prominent in M-type, very weak in S-type and absent in carbon stars as all oxygen is locked up in CO. No C_2 band at 1.77 μm is seen here as observed in carbon-rich Miras.

The K band spectra are shown in the most bottom panel of Fig. 4. The ^{12}CO first overtone series at 2.2935, 2.3227 μm , neutral atomic lines of Na I doublet at 2.20 μm , Ca I triplet at 2.26 μm are seen in our spectra, which are original features in M-type evolved stars ([Rayner et al. 2009](#)). The $^{12}\text{CO}(2,0)$ first overtone band heads are the strongest absorption feature in K band in cool stars, and its strength depends on both luminosity and effective temperature ([Ramirez et al. 1997](#); [Cesetti et al. 2013](#)). The first overtone of ^{13}CO is also visible in our spectra, though its strength is relatively weak compared to ^{12}CO first overtone series.

The $\text{H}\alpha$ emission line is seen only at phase ~ 0.43 . The $\text{Pa}\beta$ emission line appears in two visual phase 1.83

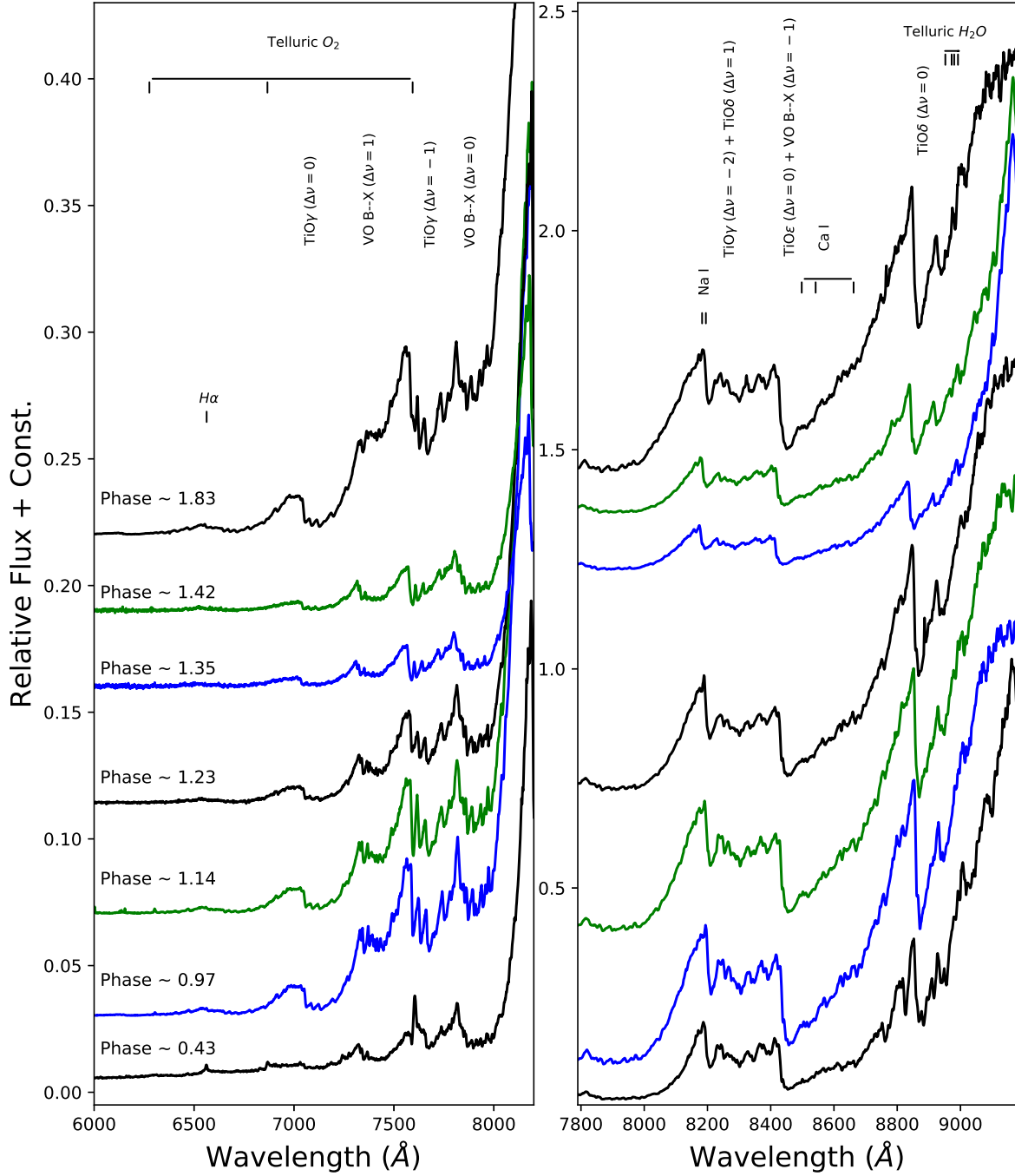


Figure 3. In top two panels, the optical spectra of the object in the range 6000–9200 Å, which show visible features of TiO and VO bands at different phases of the Mira including H α emission at phase 0.43. The spectra have been normalized to unity at 9165 Å, and offset by constant values 0.0, 0.03, 0.07, 0.11, 0.16, 0.19, 0.22 (left panel) and 0.0, 0.06, 0.36, 0.70, 1.20, 1.35, 1.40 (right panel) respectively with respect to the bottom-most spectra.

and 1.92. The $\text{Br}\gamma$ appears at phase 1.83 and reach maximum intensity at 1.92. These emission lines appear in the spectra due to shock wave generation in the Mira atmosphere. It is to be noted that $\text{H}\alpha$ is seen at phase 0.43, while $\text{Pa}\beta$ and $\text{Br}\gamma$ are seen near maximum phase. While other studies find Balmer lines usually around maximum phase (e.g., Fox et al. 1984; Fox & Wood 1985).

The overall low-resolution continuum shape of J, H and K spectra turn downwards at the end of the band indicating absorption due to broad H_2O absorption features centered at $1.4\ \mu\text{m}$, $1.9\ \mu\text{m}$ & $2.7\ \mu\text{m}$ in our spectral coverage (Rayner et al. 2009). It is strongly visible that the continuum shape is changing over the variability phases.

3.5.1. Phase dependent spectral variability

The variation in the absorption depth of TiO and VO with T_{eff} is well documented from long before (Merrill 1962). Lockwood (1972) found that TiO band-strength indices decrease in stars later than M7, and it saturates in M9 Miras. We explore the phase variation of $[\text{TiO}]_2$ index centered at $7100\ \text{\AA}$ as described in O’Connell (1973). But, $[\text{TiO}]_2$ index shows no significant variation over the phase. It is to be noted that we consider here the optical phase variation.

Another triple-headed absorption bands of TiO at 8433, 8442, 8452 \AA , $[\text{TiO}]_3$, are considered following Zhu et al. (1999) for such phase variation studies. The $[\text{TiO}]_3$ is defined as,

$$[\text{TiO}]_3 = -2.5 \log\left(\frac{F_\lambda}{F_C}\right) \quad (4)$$

where, F_λ is flux at λ and F_C is the interpolated continuum at λ . The pseudo continuum was generated in the left window of the band at $8390 - 8410\ \text{\AA}$, and right windows at $8700 - 8725\ \text{\AA}$. Then the spectrum is normalized by the continuum, and the $\frac{F_\lambda}{F_C}$ is measured in the range $8455 - 8470\ \text{\AA}$. As shown in Fig. 5, the $[\text{TiO}]_3$ index shows significant variation with the pulsation phase, it increases as the visual brightness decreases, becomes constant at certain phases (saturation effect), and then further decreases with visual brightness increases.

The Fig. 3 shows three strong absorption bands 706-724 nm (band1), 770-807 nm (band2) and 829-857 nm (band3), which are related to spectral types of static giants (Fluks et al. 1994). The flux ratio at different bands is defined by Fluks et al. (1994). We studied the flux ratio at those bands and found that the band2 to band3 ratio (as $S_{2/3,Sp}$) show pronounce variation with phase as shown in the Fig. 5. The $S_{2/3,Sp}$ becomes maximum at visual maximum while minimum at a visual minimum.

We have measured the equivalent widths (EWs) for the atomic spectral Na I at $2.206\ \mu\text{m}$, Ca I at $2.263\ \mu\text{m}$. The continuum bands for Na I and Ca I are taken from Ramirez et al. (1997) and mentioned in Table 4. The spectra were normalized by the local pseudo-continuum, and EWs of the particular atomic features were estimated by using splot task in the IRAF by fitting a Gaussian function to each feature. The Na doublet is present in the $2.2051 - 2.2099\ \mu\text{m}$ region but blended with metallic lines like Si I ($2.2069\ \mu\text{m}$), Sc I (2.2058 and $2.2071\ \mu\text{m}$) and V I ($2.2097\ \mu\text{m}$) in our low-resolution spectra. The Ca triplet appear in the $2.2609 - 2.2665\ \mu\text{m}$ regions, and is very sensitive to temperature. The 3rd and 4th panels of Fig. 5 show their phase variation. The atomic lines, in particular, are weak features that are very difficult to measure in low-resolution spectra, and no significant trends with phase are apparent, except possibly for Ca.

In the $1.5 - 2.4\ \mu\text{m}$ region, the first-overtone ($\Delta\nu=2$) and the CO second overtone ($\Delta\nu=3$) band heads of CO are the dominant features in the spectra as mentioned in the earlier section. We studied the phase dependent variations of these 2-0 (first overtone) and 3-0, 4-1, 5-2, 6-3 (second overtone) ^{12}CO band heads. We estimated the EWs of CO at different phase considering the local continuum as mentioned in the Table 4, the continuum has been fitted with first order spline fitting function (linear interpolation) at peak points. We estimated the EWs of CO at different phase as shown in Fig. 5. The EWs of 3-0 and 4-1 band heads doesn’t demonstrate any significant change during the pulsation cycle. The EWs of 2-0 first overtone band change significantly. The EWs of 5-2 and 6-3 band heads showed weak variation. The result should be taken as a caution as such small variation might occur due to the computational artifact, continuum selection and blending effect from the weak OH-lines. The shock wave, in general, propagates through the Mira atmosphere (CO first overtone forming-layer) in between optical phase $\sim 0.1 - 0.2$, which alters velocity profile known from high-resolution spectra (Hinkle & Barnes 1979b; Nowotny et al. 2010). Even in our low to intermediate resolution spectra, the CO absorption features appear to change in Fig. 6. It is expected that the combination of modified individual lines will also modify the shape of the band as a whole.

The shape of NIR spectra in Miras is dominated by strong, and broad water bands centered at $1.4\ \mu\text{m}$ and $1.9\ \mu\text{m}$ and $2.7\ \mu\text{m}$ regions (Johnson et al. 1968). The depth of water bands vary with Mira phases and become strongest at minimum light (Strecker et al. 1978). Due to this water absorption, the H and K-band spectra bend downward at the end of both bands. So, the curvature of

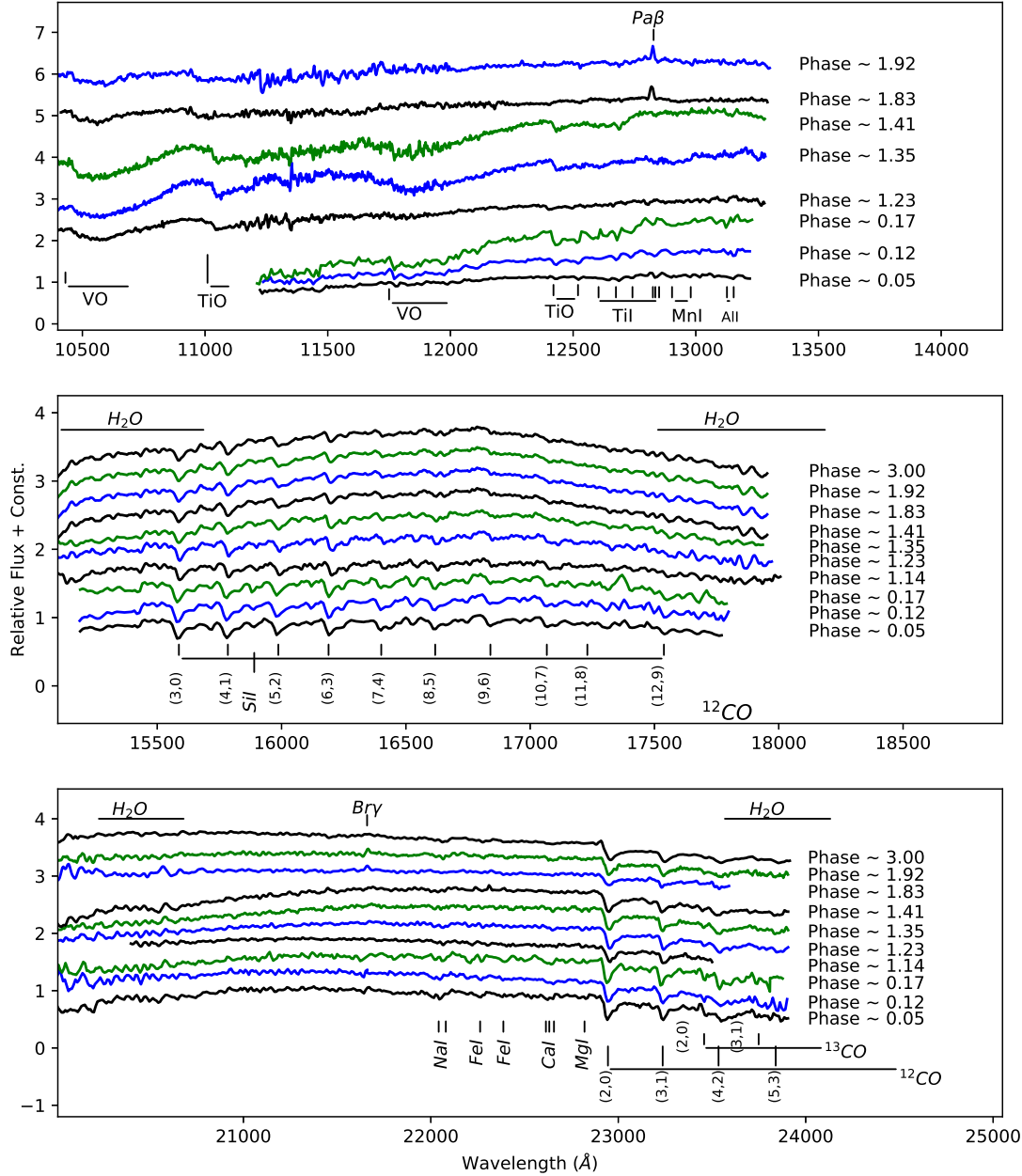


Figure 4. The NIR JHK-band spectra in the wavelength range 1.02–2.39 μm at eight different phases of the Mira are shown here in the 1st, 2nd, and 3rd panels, respectively. First three NIR spectra from the bottom (phase ~ 0.05 , 0.12, 0.17) are taken with the NICMOS-3 instrument on 1.2m Mt.Abu telescope, and rest are observed with TIRSPEC instrument on 2.0m HCT. In J-band, molecular bands like TiO, VO, and few atomic lines are present in the spectra. The Pa β emission line appears at two phases (1.83 and 1.92). The H-band spectra in the wavelength range 1.52–1.80 μm show strong four ¹²CO second overtone bands including several OH lines. In the K-band spectra, the ¹²CO first overtone bands are dominated features in the spectra, and Na I and Ca I are seen at 2.20 μm and 2.26 μm , respectively. The Br γ (at 2.16 μm) emission line appears at phases (1.83, 1.92 and likely at 0.05). The spectra have been normalized to unity at 12000 Å (J-band), 16500 Å (H-band), 21700 Å (K-band), and offset by constant values 0.0, 0.30, 0.60, 0.11, 1.70, 2.40, 3.30, 4.20, 5.10 (1st panel) respectively with respect to the bottom-most spectra of the same panel (J-band), and 0.30 to each spectrum of H and K-band).

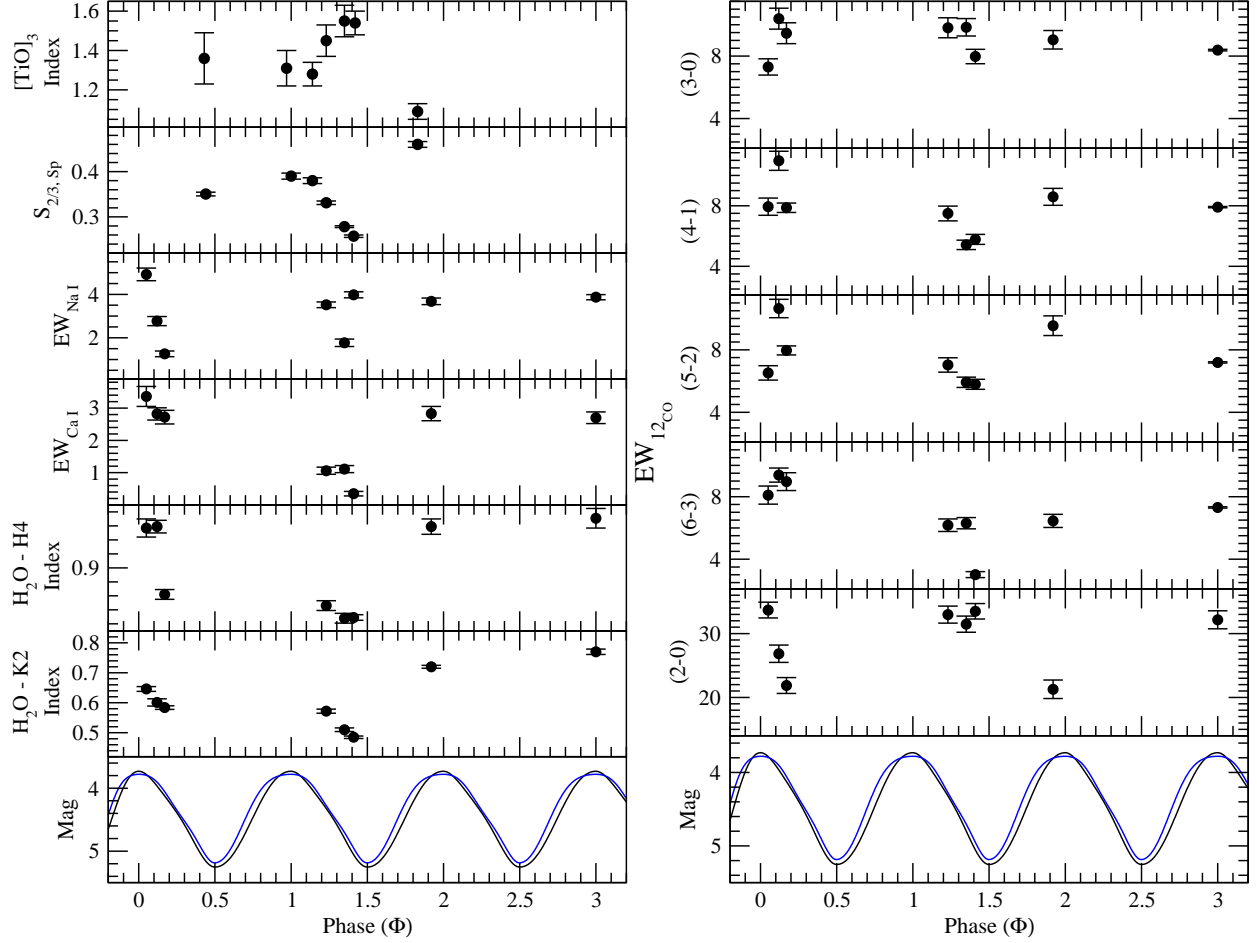


Figure 5. The phase variation of $[\text{TiO}]_3$, $S_{2/3,Sp}$, Na I, Ca I, $\text{H}_2\text{O}-\text{K}2$ equivalent width/index are shown with the visual phase. The bottom panel shows the K-light curve (black) and I-light curve (scaled with K-light curve).

the spectral changes depending on the water absorption. To quantify water absorption in our data, we measured the $\text{H}_2\text{O}-\text{H}4$ and $\text{H}_2\text{O}-\text{K}2$ indices, which shows the curvature variation of the spectra. The $\text{H}_2\text{O}-\text{K}2$ Index is taken from [Rojas-Ayala et al. \(2012\)](#) as,

$$H_2O - K2 = \frac{\langle F(2.070 - 2.090) \rangle / \langle F(2.235 - 2.255) \rangle}{\langle F(2.235 - 2.255) \rangle / \langle F(2.360 - 2.380) \rangle} \quad (5)$$

Where $\langle F(a - b) \rangle$ represents the median flux level in the wavelength range defined by a and b in μm . [Rojas-Ayala et al. \(2012\)](#) calculated this index for M and K-type dwarfs. Here that same index is explored using the spectra for M-type giants in the wavelength range of $2.07\mu\text{m}$ to $2.38\mu\text{m}$.

For the H-band spectra, several authors defined spectro-photometric indices to measure water absorption (e.g., [Allers et al. 2007](#); [Weights et al. 2009](#); [Scholz et al. 2012](#)). Here we define a new $\text{H}_2\text{O}-\text{H}4$ index as,

$$H_2O - H4 = \frac{\langle F(1.531 - 1.541) \rangle / \langle F(1.670 - 1.690) \rangle}{\langle F(1.670 - 1.690) \rangle / \langle F(1.742 - 1.752) \rangle} \quad (6)$$

where $\langle F(a - b) \rangle$ represents the median flux level in the wavelength range defined by a and b in μm .

In Fig. 5, the phase variation of these two $\text{H}_2\text{O}-\text{H}4$ and $\text{H}_2\text{O}-\text{K}2$ indices are shown. The smaller value of H_2O indices in H and K corresponds to greater amounts of H_2O opacity. The significant variations of these indices apparent in the Fig. 5. In Fig. 5, we see that $\text{H}_2\text{O}-\text{H}4$ and $\text{H}_2\text{O}-\text{K}2$ indices show significant variation with the pulsation cycles, the value of indices are strongest at visual maximum while weak at a visual minimum i.e. H_2O opacity is stronger at visual minimum. Our result confirms the trends already seen by [Strecker et al. \(1978\)](#).

3.5.2. Spectral type

The depth of triple-headed absorption band of TiO (8432, 8442 and 8452 \AA) at the optical spectra is excel-

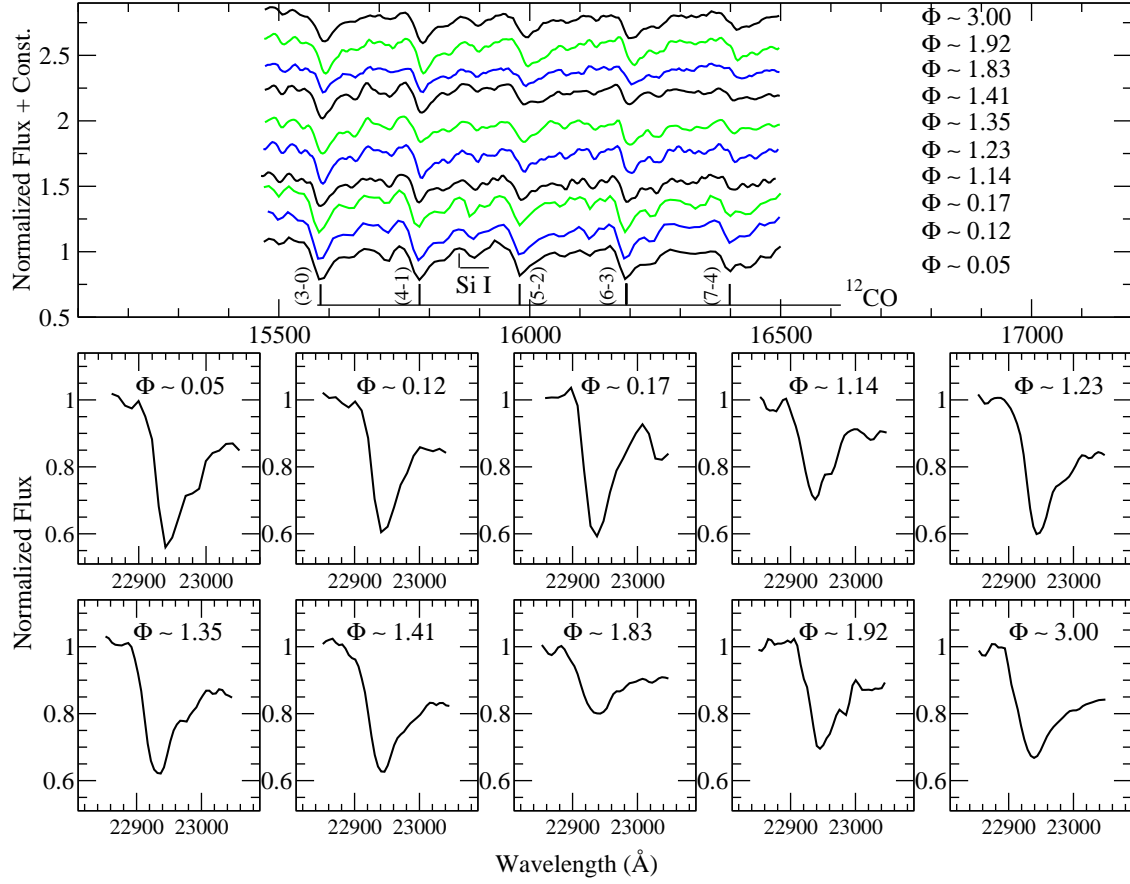


Figure 6. The changing shape of CO-second overtones and one CO first overtone at 2.29 μm with phases are shown here

Table 4. Definitions of Spectral Bands

Feature	Bandpass (μm)	Continuum bandpass (μm)	Ref
[TiO] ₃	0.8455-0.8725	0.8390-0.8410, 0.8700-0.8725	1
Na I	2.204-2.211	2.191-2.197, 2.213-2.217	2
Ca I	2.258-2.269	2.245-2.256, 2.270-2.272	2
¹² CO(3-0)	1.5550-1.5625	-	2
¹² CO(4-1)	1.5752-1.5812	-	2
¹² CO(5-2)	1.5952-1.6020	-	2
¹² CO(6-3)	1.6170-1.6220	-	2
¹² CO(2-0)	2.289-2.302	2.270-2.272, 2.275-2.278 2.282-2.286, 2.288-2.289	2

¹Zhu et al. (1999); ²Ramirez et al. (1997).

Table 5. Phase Dependent Study

Date of Obs.	Optical Phase	$[TiO]_3$ Index	$S_{2/3,Sp}$	Na I 2.20 μm	CaI 2.26 μm	CO 3-0	CO 4-1	CO 5-2	CO 6-3	CO 2-0	H_2O -H4 Index	H_2O -K2 Index	Sp. <i>Type</i> ¹
2013 Mar 21.99	0.05	-	-	4.92±0.29	3.36±0.31	7.30±0.52	7.94±0.57	6.52±0.46	8.1±0.58	33.68±1.23	0.96±0.01	0.65±0.01	-
2013 Apr 29.99	0.12	-	-	2.77±0.21	2.82±0.19	10.39±0.67	10.97±0.63	10.64±0.59	9.38±0.45	26.84±1.36	0.96±0.01	0.60±0.01	-
2013 May 30.95	0.17	-	-	1.26±0.13	2.72±0.21	9.46±0.67	7.87±0.31	7.96±0.29	8.96±0.57	21.87±1.24	0.86±0.01	0.58±0.01	-
2013 Oct 15.57	0.44	1.36±0.13	0.350 ± 0.004	-	-	-	-	-	-	-	-	-	M9.5
2014 May 21.91	1.0	1.31±0.09	0.390 ±0.007	-	-	-	-	-	-	-	-	-	M9
2014 Aug 18.72	1.14	-	-	1.37±0.11	1.10±0.12	8.03±0.44	6.02±0.33	6.22±0.34	6.023±0.32	18.65±1.08	0.90±0.011	-	-
2014 Aug 19.83	1.14	1.28±0.06	0.380±0.006	-	-	-	-	-	-	-	-	-	M9
2014 Oct 06.73	1.23	1.45±0.08	0.331 ±0.003	3.52±0.13	1.06±0.11	9.81±0.64	7.49±0.49	7.03±0.46	6.173±0.40	32.97±1.33	0.85±0.01	0.57±0.01	M9
2014 Dec 12.55	1.35	1.55±0.08	0.278 ±0.002	1.77±0.17	1.11±0.11	9.84±0.56	5.42±0.31	5.92±0.33	6.30±0.36	31.47±1.27	0.83±0.01	0.51±0.01	M10
2015 Jan 13.58	1.41	-	-	3.98±0.14	0.35±0.07	7.97±0.46	5.78±0.33	5.788±0.32	3.01±0.19	33.49±1.21	0.83±0.01	0.48±0.01	-
2015 Jan 18.56	1.41	1.54±0.06	0.257 ±0.003	-	-	-	-	-	-	-	-	-	M10
2015 July 05.79	1.83	1.09±0.04	0.460 ±0.006	1.94±0.09	1.57±0.17	6.85±0.31	6.66±0.30	6.03±0.27	4.32±0.20	19.52±0.93	0.93±0.01	-	M8.5
2015 Aug 11.88	1.92	-	-	3.68±0.15	2.83±0.22	9.04±0.59	8.59±0.56	9.54±0.63	6.45±0.42	21.27±1.45	0.96±0.01	0.72±0.01	-
2016 Dec 19.54	3.00	-	-	3.87±0.12	2.70±0.18	8.38±0.05	7.91±0.04	7.19±0.04	7.31±0.04	32.15±1.41	0.97±0.01	0.77±0.01	-

¹The spectral type has been estimated using the correlation with $[TiO]_3$ Index

lent spectral type indicator. Following [Zhu et al. \(1999\)](#), we estimate the spectral type (ST) of the object at different variability phase, which is defined as the $[TiO]_3$ index ($[TiO]$ at 8450 Å).

$$ST = 2.43 + 6.65[TiO]_3 - 1.12[TiO]_3^2 \quad (7)$$

We have measured $[TiO]_3$ index using Eqn. 4 from the spectra as described in the earlier section 3.5.1, the ST is estimated using the above relation in Eqn. 7, and the STs at different phases are shown the Table 5. The ST of the object varies from M8.5 to M10 over the phase of the pulsation cycle in our limited phase coverage. The saturation effect of $[TiO]_3$ is problematic to estimate the STs over phases as described in the earlier section 3.5.1.

4. SUMMARY AND CONCLUSION

From long-term optical/NIR photometric and spectroscopic observations, we have characterized the MASTER OT J2124+32. Our main results are summarized as follows :

1. From the best-fit of optical/NIR light curves, we estimated the variability period of the object as 465 ± 30 days. The strong wavelength-dependent variability amplitudes in optical to NIR wavelengths are observed as $\Delta I \sim 4$ mag, ΔC (400–900 nm) ~ 3.4 mag, $\Delta J \sim 2.2$ mag, $\Delta H \sim 1.9$ mag and $\Delta K \sim 1.5$ mag. Such large periods and strong wavelength-dependent variability amplitude are seen in Miras only. Interestingly, a phase lag of ~ 60 days between the optical and NIR light curves like a Mira variable is also seen. Large (J-K) NIR colors varying 1.78–3.0 mag over phases, signifies that it is a red object like cool Miras.
2. From Period-Luminosity (PL) relation, the distance to the source is estimated as 3.27 ± 0.02 kpc. The absolute bolometric magnitude is determined as -5.29 ± 0.38 mag, corresponding to the luminosity of $\sim 10,250 L_\odot$.
3. Using DUSTY based MoD code, we have done the SED fitting the NIR to Far-IR data. The best fit SED of all photometric measurements provides

an effective temperature of 2800 K, and dust shell temperature 1248 K. The SED provides luminosity of the object $9282 L_\odot$, which is comparable to the P-L based estimation, and mass-loss rate of $0.7 \times 10^{-6} M_\odot yr^{-1}$.

4. From Optical/NIR spectra, we find that the source has all kind spectral signatures of a cool M-type star. The spectral features indicate an O-rich Mira as it shows most prominent feature of VO band and TiO bands. We rule out S- or C-type nature as ZrO bands at 1.03 and 1.06 μm and C_2 band head at 1.77 μm are absent.
5. The phase-dependent of optical/NIR spectral features are studied. Notable variable features in all atomic and molecular lines (e.g., TiO, Ca I, H_2O and CO bands) over phases are seen here like commonly observed in Miras. Our optical spectral data show an apparent variation of the spectral type of the object over the pulsation cycle.

In conclusion, all these observational properties of the object J2124+32 confirms a new O-rich Mira variable toward the Cygnus.

ACKNOWLEDGEMENTS

The authors are very much thankful to the anonymous referee for his/her critical and valuable comments, which help us to improve the paper. This research work is supported by S N Bose National Centre for Basic Sciences under Department of Science and Technology, Govt. of India. The authors are thankful to the HTAC members and staff of HCT, operated by Indian Institute of Astrophysics (Bangalore); staff of the Mt. Abu observatory, operated by Physical Research Laboratory (Ahmedabad). SG is thankful to M. A. T. Groenewegen for helpful discussions and valuable suggestions on DUSTY code and MoD.

Software: starlink ([Currie et al. 2014](#)), IRAF (Tody 1986, Tody 1993), TIRSPEC pipe-line ([Ninan et al. 2014](#)), PERIOD044 ([Lenz & Breger 2005](#)), More of Dusty (MoD; [Groenewegen 2012](#)), DUSTY ([Ivezić & Elitzur 1997](#)), MARCS ([Gustafsson et al. 2008](#))

REFERENCES

- | | |
|--|--|
| <p>Allers, K. N., Jaffe, D. T., Luhman, K. L., et al. 2007, ApJ, 657, 511</p> <p>Alvarez, R., Jorissen, A., Plez, B., et al. 2000, A&A, 362, 655</p> | <p>Aringer, B., Girardi, L., Nowotny, W., et al. 2009, A&A, 503, 913</p> <p>Bessell, M. S., Brett, J. M., Wood, P. R., Scholz, M., 1989, A&A, 213, 209</p> |
|--|--|

- Bessell, M. S., Scholz, M., Wood, P. R., 1996, *A&A*, 307, 481
- Bessell, M. S., Castelli, F., Plez, B., 1998, *A&A*, 333, 231
- Bieging et al. 2002, *A&A* 384, 965
- Castelaz, M. W. & Luttermoser, D. G. 1997, *AJ*, 114, 1584
- Castelaz, M. W. et al., 2000, *AJ*, 120, 2627
- Cesetti, M., Pizzella, A., Ivanov, V. D., et al. 2013, *A&A*, 549, 129
- Currie, M. J.; Berry, D. S.; Jenness, T.; Gibb, A. G.; Bell, G. S.; Draper, P. W., 2014, *ASPC*, 485, 391
- Cutri, R. M., et al. 2003, *yCat*, 2246, 0
- Cutri, R. M., et al. 2013, *yCat*, 2328, 0
- Dejonghe, H., van Caelenberg, K. 1999, *IAUS*, 191, 501
- Eggen, O. J., 1998, *AJ*, 115, 2435
- Feast, M. W., Glass, I. S., Whitelock, P. A., Catchpole, R. M., 1989, *MNRAS*, 241, 375
- Fleischer, A. J., Gauger, A., Sedlmayr, E. 1992, *A&A*, 266, 321
- Fluks, M. A.; Plez, B.; The, P. S., et al. 1994, *A&AS*, 105, 311
- Fox, M. W., Wood, P. R., Dopita, M. A., 1984, *ApJ*, 286, 337
- Fox, M. W., Wood, P. R., 1985, *ApJ*, 297, 455
- Gautschi-Loidl, R., Höfner, S., Jørgensen, U. G., Hron, J. 2004, *A&A*, 422, 289
- Groenewegen, M. A. T., Lançon, A., Marescaux, M. 2009, *A & A*, 504, 1031
- Groenewegen, M. A. T., 2012, *A&A*, 543, 36
- Guha Niyogi, Suklima, Speck, Angela K., Onaka, T., 2011, *ApJ*, 733, 93
- Gustafsson, B., Edvardsson, B., Eriksson, K., et al. 2008, *A & A*, 486, 951
- Habing, H. J. 1988, *A&A*, 200, 40
- Habing, H. J. 1996, *A&AR*, 7, 97
- Hambsch, F. -J. 2012, *JAAVSO*, 40, 1003
- Herwig, F. 2005, *ARA&A*, 43, 435
- Hinkle, K. H. 1978, *ApJ*, 220, 210
- Hinkle, K. H., Barnes, T. G. 1979, *ApJ*, 227, 923
- Hinkle, K. H., Barnes, T. G. 1979, *ApJ*, 234, 548
- Hinkle, K. H., Hall, D. N. B., Ridgway, S. T., 1982, *ApJ*, 252, 697
- Hinkle, Kenneth H., Wilson, Teresa D., Scharlach, Werner W. G., Fekel, Francis C., 1989, *AJ*, 98, 1820
- Höfner, S., Jørgensen, U. G., Loidl, R., Aringer, B. 1998, *A&A*, 340, 497
- Hughes, Shaun M. G., Wood, Peter R., 1990, *AJ*, 99, 784
- Ireland, M. J., Scholz, M., Wood, P. R., 2004, *MNRAS*, 352, 318
- Ita, Y., Tanabé, T., Matsunaga, N., et al., 2004, *MNRAS*, 353, 705
- Ita, Y., Matsunaga, N., 2011, *MNRAS*, 412, 2345
- Ishihara, D., Onaka, T., Kataza, H., et al., 2010, *A&A*, 514A, 1
- Ivezić, Ž., Elitzur, M., 1997, *MNRAS*, 287, 799
- Ivezić, Ž., Elitzur, M., 1999, *DUSTY* user manual, University of Kentucky internal report
- Johnson, H. L., Coleman, I., Mitchell, R. I., Steinmetz, D. L., 1968, *CoLPL*, 7, 83
- Jura, M., & Kleinmann, S. G. 1990, *ApJ*, 364, 663
- Jura, M., & Kleinmann, S. G. 1992, *ApJS*, 79, 105
- Jurić, M., Ivezić, Ž., Brooks, A., et al. 2008, *ApJ*, 673, 864
- Keeley, D. A., 1970, *ApJ*, 161, 657
- Kharchenko, N., Kilpio, E., Malkov, O., Schilbach, E., 2002, *A&A*, 384, 925
- Lançon, A., Mouhcine, M., Fioc, M., Silva, D. 1999, *A&A*, 344, 21
- Lançon, A., & Wood, P. R., 2000, *A&AS*, 146, 217
- Lançon, A., Hauschildt, P. H., Ladjal, D., Mouhcine, M., 2007, *A&A*, 468, 205
- Lebzelter, Th., Hinkle, Kenneth H., Hron, J., 1999, *A&A*, 341, 224
- Le Bertre, T., 1992, *A&AS*, 94, 377
- Lenz, P., Breger, M. 2005, *CoAst*, 146, 53
- Lipunov, V., Gorbovskoy, E., Afanasiev, V., et al. 2016, *A&A*, 588, 90
- Lipunov, V. M., Kornilov, V., Gorbovskoy, E., et al. 2017, *MNRAS*, 465, 3656
- Lockwood, G. W., 1972, *ApJS*, 24, 375
- Loidl, R., Höfner, S., Jørgensen, U. G., Aringer, B. 1999, *A&A*, 342, 531
- Lomb, N. R., 1976, *Ap&SS*, 39, 447
- Mattei, J. A., 1997, *JAAVSO*, 25, 57
- Merrill, Paul W., Deutsch, Armin J., Keenan, Philip C. 1962, *ApJ*, 136, 21
- Mondal, Soumen, Chandrasekhar, T., 2005, *AJ*, 130, 842
- Mondal, S., Lin, C. C., Chen, W. P., et al, 2010, *AJ*, 139, 2026
- Mondal, S., Das, R. K., Ashok, N. M., Banerjee, D. P. K., Dutta, S., Ghosh, S., Mondal, A., 2013, *ATel*, #4931
- Ninan, J. P., Ojha, D. K., Ghosh, S. K., et al., 2014, *Journal of Astronomical Instrumentation*, 3, 1450006
- Ngeow Chow-Choong, Lucchini S., Kanbur S., Barrett B., Lin B., 2013, *arXiv:1309.4297 [astro-ph.SR]*
- Nowotny, W., Aringer, B., Höfner, S., Gautschi-Loidl, R., Windsteig, W. 2005, *A&A*, 437, 273
- Nowotny, W., Lebzelter, T., Hron, J., Höfner, S. 2005, *A&A*, 437, 285
- Nowotny, W., Höfner, S., Aringer, B. 2010, *A&A*, 514A, 35N
- O'Connell, R. W., 1973, *AJ*, 78, 1074

- Olofsson, H. 2004, in *Asymptotic Giant Branch Stars*, ed. H. J. Habing, & H. Olofsson (Springer), Chap. 7, 325
- Perrin, G., Ridgway, S. T., Mennesson, B., et al., 2004, *A&A*, 426, 279
- Ramirez, S. V., Depoy, D. L., Frogel, Jay A., Sellgren, K., Blum, R. D., 1997, *AJ*, 113, 1411
- Rayner, John T., Cushing, Michael C., Vacca, William D., 2009, *ApJS*, 185, 289
- Reid M. J., Goldston J. E., 2002, *ApJ*, 568, 931
- Rojas-Ayala, Brbara, Covey, Kevin R., Muirhead, Philip S., Lloyd, James P., 2012, *ApJ*, 748, 93R
- Scargle, J. D., 1982, *ApJ*, 263, 835S
- Schlafly, Edward F., Finkbeiner, Douglas P., 2011, *ApJ*, 737, 103
- Schlegel, David J., Finkbeiner, D. P., Davis, M., 1998, *ApJ*, 500, 525
- Scholz, A., Muzic, K., Geers, V., et al., 2012, *ApJ*, 744, 6
- Smith, B. J., Leisawitz, D., Castelaz, M. W., Luttermoser, Donald, 2002, *AJ*, 123, 948
- Smith, B. J., Price, S. D., Moffett, A. J., 2006, *AJ*, 131, 612
- Soszyński, I., Udalski, A., Poleski, R., Kozłowski, S., Wyrzykowski, L., Pietrukowicz, P., Szymański, M. K., Kubiak, M., Pietrzyński, G., Ulaczyk, K., Skowron, J., 2012, *AcA*, 62, 219
- Strecker, D. W., Erickson, E. F., Witteborn, F. C., 1978, *AJ*, 83, 26
- Tej, A., Lançn, A., Scholz, M. & Wood, P. R. 2003a, *A&A*, 412, 481
- Tej, A., Lançn, A. & Scholz, M. 2003b, *A&A*, 401, 347
- Tiurina, N. et al., 2013, *#ATel*, 4888
- Thompson, R. R., Creech-Eakman, M. J., van Belle, G. T. 2002, *ApJ*, 577, 447T
- Tsuji, T. 2009, *A&A*, 504, 543
- Wallace, L., Hinkle, K., 1996, *ApJS*, 107, 312
- Weights, D. J., Lucas, P. W., Roche, P. F., Pinfield, D. J., Riddick, F., 2009, *MNRAS*, 392, 817
- Whitelock, P., Marang, F., Feast, M., 2000, *MNRAS*, 319, 728
- Whitelock, Patricia A., Feast, M. W., van Loon, Jacco Th., Zijlstra, Albert A., 2003, *MNRAS*, 342, 86W
- Whitelock, Patricia A., Feast, Michael W., van Leeuwen, Floor, 2008, *MNRAS*, 386, 313W
- Winters, J. M., Fleischer, A. J., Le Bertre, T., Sedlmayr, E., 1997, *A&A*, 326, 305
- Winters, J. M., Le Bertre, T., Jeong, K. S., Helling, Ch., Sedlmayr, E. 2000, *A&A* 361, 641
- Wittkowski, M., Boboltz, D. A., Ohnaka, K., Driebe, T., Scholz, M. 2007, *A&A*, 470, 191
- Wittkowski, M., Boboltz, D. A., Driebe, T., Le Bouquin, J.-B., Millour, F., Ohnaka, K., Scholz, M. 2008, *A&A*, 479, 21
- Wood, P. R., Sebo, K. M., 1996, *MNRAS*, 282, 958
- Wood, P. R., Alcock, C., Allsman, R. A., et al. 1999, *IAUS*, 191, 151
- Wright, N. J., Barlow, M. J., Greimel, R., Drew, J. E., Matsuura, M., Unruh, Y. C., Zijlstra, A. A., 2009, *MNRAS*, 400, 1413
- Zhu, Z. X., Friedjung, M., Zhao, G., Hang, H. R., Huang, C. C., 1999, *A&AS*, 140, 69